AGU PUBLICATIONS

Journal of Advances in Modeling Earth Systems

RESEARCH ARTICLE
10.1002/2014MS000314

Key Points:
- The larger the shear, the longer it takes the TCs to form and intensify
- Shear affects development of TCs through modulating convective intensity and spatial distribution
- Higher SST and moisture allow TCs to form faster and resist stronger shear

Correspondence to:
F. Zhang,
fzhang@psu.edu

Citation:
Tao, D., and F. Zhang (2014), Effect of environmental shear, sea-surface temperature, and ambient moisture on the formation and predictability of tropical cyclones: An ensemble-mean perspective. *J. Adv. Model. Earth Syst.*, *06*, doi:10.1002/2014MS000314.

Received 13 FEB 2014
Accepted 17 APR 2014
Accepted article online 22 APR 2014

Effect of environmental shear, sea-surface temperature, and ambient moisture on the formation and predictability of tropical cyclones: An ensemble-mean perspective

Dandan Tao[1] and Fuqing Zhang[1]

[1]Department of Meteorology, Pennsylvania State University, University Park, Pennsylvania, USA

Abstract The formation and predictability of sheared tropical cyclones (TCs) are explored through a series of convection-permitting ensemble simulations using the Weather Research and Forecasting (WRF) model with different environmental vertical wind shear, sea-surface temperature (SST), and ambient moisture conditions. Small-amplitude random moisture perturbations are introduced in the lower troposphere as the initial-condition uncertainties to generate the ensembles under different environmental conditions; the composites of each ensemble are analyzed in this study to examine the mean dynamics of sheared TCs. It is found that the environmental shear can significantly affect the timing of tropical cyclone formation by influencing the spatial distribution of convection and subsequently changing the positive feedback between diabatic heating and the TC vortex primary circulation. Except for the initial spin-up periods, the larger the vertical wind shear, the farther and weaker the convection from the TC center, which leads to a weakening TC vortex circulation and more time is needed to start the onset of rapid intensification (RI). The simulated tropical cyclones cannot start rapid intensification during a 9 day simulation if the shear exceeds 7.5 m/s for a constant SST of 27°C. Increasing SST to 29°C reduces the tilt magnitude and thus shortens the RI onset time because of the increased diabatic heating closer to the TC center. Reduction in the environmental moisture content will eventually lead to weakened convection and delayed or failed precession in the latter stages if the TC forms at all. In summary, the development of tropical cyclones is largely depending on the magnitude of vertical wind shear and diabatic heating, which can be further altered by other environmental conditions, such as the sea-surface temperature and ambient moisture content.

1. Introduction

Tropical cyclone intensity forecasting has been a big challenge for both forecasters and researchers. Many studies have focused on the internal dynamics of TCs in order to improve the understanding of tropical cyclone inner-core evolution and advance possible methods to increase intensity forecast accuracy. It is revealed that the limited predictability of random, chaotic moist convection may ultimately limit the predictability of tropical cyclones; even very small and virtually unnoticeable differences in the initial conditions can dramatically alter the development of a TC [e.g., *Sippel and Zhang*, 2008, 2010; *Nguyen et al*., 2008; *Zhang and Sippel*, 2009; *Munsell et al*., 2013]. This limitation is even more apparent under moderate vertical wind shear conditions [*Zhang and Tao*, 2013].

The role of vertical wind shear on TC evolution has been extensively explored both in observational studies [e.g., *Gray*, 1968; *Corbosiero and Molinari*, 2002; *Davis and Ahijevych*, 2012] and in numerical and theoretical works [*Jones*, 1995; *DeMaria*, 1996; *Frank and Ritchie*, 1999; *Reasor and Montgomery*, 2001; *Tang and Emanual*, 2010; *Rappin and Nolan*, 2012; *Stern and Zhang*, 2013]. *Jones* [1995, 2004] used a dry model to diagnose the initial downshear tilt of the vortex. In her papers, she recognized that there is a wave number-1 vertical motion asymmetry that develops to produce a potential-vorticity anomaly that can help the vortex to achieve flow balance. Although the dry dynamics can explain part of the shear-induced phenomena in TC development, the diabatic and moist processes introduce much more complexity to the subsequent TC evolution [*Wang and Holland*, 1996; *Riemer et al*., 2010; *Nolan and Rappin*, 2008; *Rappin and Nolan*, 2012; *Ge et al*., 2013; *Zhang and Tao*, 2013]. When convection and diabatic heating are involved, because of the asymmetry in the vertical motion, convection is suppressed on the upshear side and enhanced on the downshear side [*Marks et al*., 1992; *Franklin et al*., 1993; *Black et al*., 2002; *Chen et al*., 2006]. *Xu and Wang* [2013] pointed out that latent heat release is responsible for the balanced upward motion downshear while the

dry dynamical process contributes more to the wave number-1 asymmetry with downdraft upshear and updraft downshear. *Frank and Ritchie* [1999] showed that this convection asymmetry has a negative impact on TC genesis and intensification. They also found that the latent heating of the moist convection within the eyewall region could help to resist or even reduce the tilt of the TC vortex.

Dry air influence on the TC intensity under vertical wind shear condition is another area of active research. *Ge et al*. [2013] showed the relative location of the dry air to the right of the vertical wind shear direction is especially detrimental to a TC because the dry air is advected by the vortex circulation to the downshear side and taken into the updraft. In *Riemer et al*. [2010], the downdraft caused by precipitation flushes the midlevel dry air to the boundary layer and then this low θe air is drawn into the updraft at a downstream location, which temporarily weakens the storm. Whether the dry air can be drawn into the updraft is the most important part for the dry air intrusion.

Recent dynamical and thermodynamical studies [*Reasor and Montgomery*, 2001; *Reasor et al.,* 2004; *Rappin and Nolan*, 2012; *Zhang and Tao*, 2013] have discussed how the tilt, precession, and alignment of the TC vortex proceed under the influence of vertical wind shear. Precession is a change in the orientation of the rotational axis of a rotating body. The precession of a TC is defined as the cyclonic rotation of the tilt vector, which indicates relative motion between the upper-level and lower-level vortex centers. This phenomenon occurs as a result of the advection of anomalies by the vortex mean circulation [*Jones*, 1995], of which the mechanisms are still under debate. A weakening or maintenance of the vortex intensity is found during this process with increasing tilt magnitude. Only after alignment is it possible for the TC vortex to undergo rapid intensification [*Zhang and Tao*, 2013]. The recovery of a TC-like vortex from the adverse effects of vertical wind shear may be accelerated by the contribution of moist convection in the TC inner-core region [*Frank and Ritchie*, 1999, 2001; *Zhang and Tao*, 2013].

Though vertical wind shear has long been recognized to have a strong negative influence on the development and intensification of tropical cyclones [e.g., *DeMaria*, 1996; *Tang and Emanuel*, 2010; *Rappin and Nolan*, 2012], how this destructive effect takes place during the potential formation stages of tropical cyclones has not been thoroughly explored in the literature. The sensitivity of TC formation to the shear magnitude also remains as an open area of research. This paper uses the composites of a series of 20 member ensemble simulations to systematically analyze the behavior of a TC vortex under vertical wind shear and the differences in development given different environmental conditions (shear magnitudes, SSTs, and environmental moisture). The sensitivity of the TC formation and rapid intensification to minute, random initial moisture perturbations within each ensemble, and the intrinsic predictability of TCs will be discussed in a future publication. Since there is strong flow-dependent variability among different ensemble members within each ensemble under a given environmental condition, one unique aspect of current study is the use of ensemble-mean composites to ensure the representativeness of the findings.

Two prevailing mechanisms of vertical wind shear effect on TCs are examined. One is the midlevel dry air ventilation through boundary layer inflow [e.g., *Tang and Emanuel*, 2010; *Riemer et al*., 2010], while the other is the effect of vertical wind shear on the spatial distribution and intensity of convection and the feedback between the convection and vortex intensity, especially with respect to their influence on the vortex vertical alignment and precession.

The rest of this paper is organized as follows: section 2 gives the experimental design and the initial conditions. An overview of the composite results in our experiments is then described in section 3. The details of the two mechanisms influencing the convection strength and the feedback between the convection and vortex mean circulation are presented in section 4. The formation of the beginning 10 m wind increase is discussed in section 5. In section 6, we analyze more details under higher SST condition. Section 7 discusses the change in TC evolution when a relatively drier environment is present. Conclusions are given in section 7.

2. Experimental Design

The Advanced Version of the Weather Research and Forecast (WRF) model version 3.1 is used for all simulations. This study shares the same model setup as that in *Zhang and Tao* [2013]. All simulations are initialized

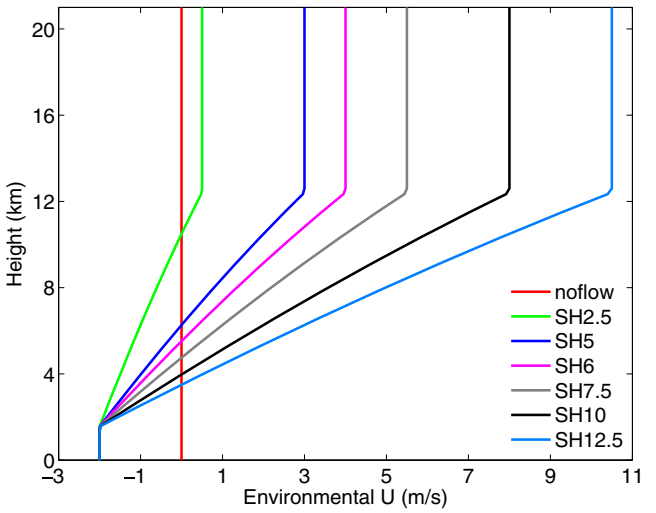

Figure 1. Vertical profiles of environmental flow for noflow, SH2.5, SH5, SH6, SH7.5, SH10, and SH12.5.

with the same idealized modified Rankine vortex but with different distributions of random low-level moisture perturbations. The vortex has a maximum surface wind speed of 15 m/s at 135 km radius. The Dunion non-SAL mean hurricane season sounding [*Dunion*, 2011] is used for the environmental moisture and temperature profile with a constant sea-surface temperature of 27°C (SST27) or 29°C (SST29) and a constant Coriolis parameter equivalent to 20°N. An additional set of dry air sensitivity experiments is also conducted to highlight the influence of a drier environment on the formation of TCs. In the dry experiments, the moisture content for all heights is kept the same within a 200 km radius, and is linearly decreased between a 200 and 300 km radius by 50%. Outside the radius of 300 km, the moisture content is reduced to 50% of its original value.

There are six sets of 20 member ensemble moist experiments under SST27, seven sets under SST29, and two sets of dry experiments under SST29. As in *Zhang and Tao* [2013], 20 sets of moisture perturbations with magnitudes randomly selected from a uniform distribution of (−0.5, 0.5) g/kg are applied to the initial moisture fields throughout the innermost domain below 950 hPa. The vertical profiles of the environmental flows for all ensemble experiments are shown in Figure 1. There is no environmental mean flow or vertical wind shear in the ensemble experiments "noflow." The other experiments (namely SH2.5, SH5, SH6, SH7.5, SH10, SH12.5) have westerly vertical wind shear of 2.5, 5, 6, 7.5, 10, and 12.5 m/s, respectively, each of which has the same surface mean easterly wind of 2 m/s. The "point-downscaling" method developed by *Nolan* [2011] is used to force the environmental vertical shear (with no temperature gradient) present in these idealized simulations. The sensitivity experiments with lower environmental moisture contents are indicated by "Dry50."

3. Overview of Composite Results

3.1. Intensity, Tilt, and Shear Evolution

The time evolution of the tropical cyclone intensity is examined in terms of the composite minimum sea level pressure (Figures 2a and 2b) and 10 m maximum wind speed (Figures 2c and 2d) by using 1 h model output from all ensemble experiments under different environmental conditions with and without vertical wind shear. In general, the larger vertical wind shear, the more time is required before the onset of RI; with the same vertical shear, the higher the SST, the faster the storm develops. The simulations with minimum vertical shear (0 or 2.5 m/s) for both SST27 and SST29 begin rapid intensification at the earliest times (at around 72 h). For SST27, the 6 m/s shear simulation does not begin RI until around 144 h while for SST29, SH6 develops only slightly (∼12 h) later than noflow or SH2.5 runs. When the shear is larger than a critical value (∼7.5 m/s under SST27, ∼12.5 m/s under SST29), the TC vortex cannot develop in the 9 day simulation window.

However, the timing of RI onset does not linearly increase with the shear magnitude. A small difference in the shear magnitude approaching the critical value can lead to large differences in the RI onset time. For example, the simulation SH2.5 with a small shear of 2.5 m/s starts RI slightly earlier than the noflow (zero shear) simulation for SST27 (Figure 2c) but not for SST29 (Figure 2d). On the other hand, increasing the shear by merely 1 m/s from SH5 to SH6 for SST27 results in a mean delay of RI by as much as 48 h (SH5-

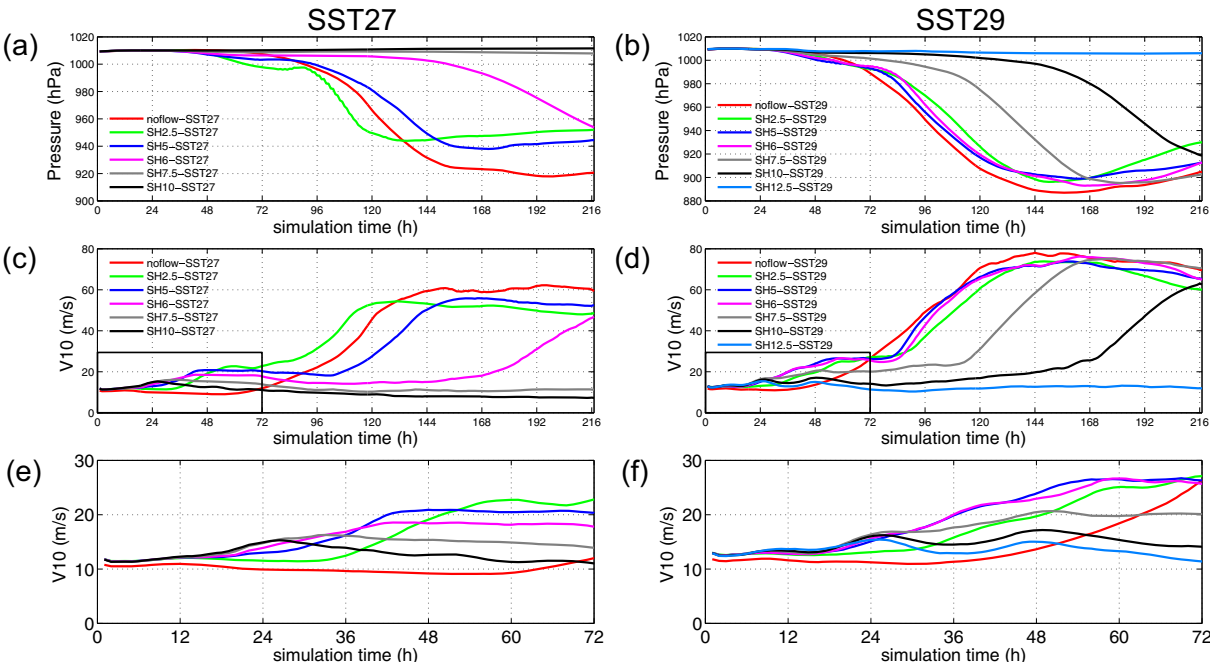

Figure 2. (a) Time evolution of minimum sea level pressure under SST27; (b) the same as Figure 2a except for SST29; (c) time evolution of maximum 10 m total wind under SST27; (d) the same as Figure 2c except for SST29; (e) highlight of the beginning 72 h evolution in Figure 2c; and (f) highlight of the beginning 72 h in Figure 2d.

SST27 and SH6-SST27 in Figures 2a and 2c). This sensitivity to shear magnitude can be especially problematic when forecasting in real time.

It should also be noted that there is an increase of the 10 m wind under all shear conditions (highlighted in Figures 3e and 3f) early in the simulations that is due to a temporal effect caused by the upward vertical motion anomaly as a result of vortex downshear tilt, which subsequently enhances the updrafts (details in section 5). It is also apparent that higher SSTs can resist higher vertical wind shear and aid in the development of TCs that do not develop under the same magnitude of large vertical wind shear under lower SSTs (details in section 6). The current study focuses on the development of TC vortices before RI happens.

To further understand how different magnitudes of vertical wind shear impact the development of the same initial vortices and to identify when these vortex columns start to differ systematically, we examine the time evolution of the direction and magnitude of the storm center tilt and the local vertical wind shear under both SST27 and SST29 conditions (Figure 3). Calculation of the tilt and shear vector is similar to that of *Rappin and Nolan* [2012] except that the weighted horizontal circulation center is used instead of the Ertel potential-vorticity center following *Zhang and Tao* [2013]. The tilt vector is calculated from the difference in the 850 and 450 hPa circulation center positions, while the local vertical shear is calculated using the difference in horizontal winds at the 850 and 450 hPa levels averaged within a 300 km radius centered on the 650 hPa circulation center (e.g., the environmental shear between these two levels in SH5-SST27 is $\sim$2 m/s initially, Figure 3c).

Though the 10 m maximum wind speeds of the sheared vortices show no sizable changes during the period after the early wind speed increase in the simulations and before the onset of RI, the vortex structure undergoes a significant transformation. For the SST27 simulations, as shown in Figures 3a and 3c, the noflow-SST27 experiments exhibit tilt and local shear magnitudes of essentially zero, which indicates that, under the no environmental flow condition, the TC vortex remains completely vertical throughout the development period and the structure of the vortex is nearly axisymmetric.

Meanwhile, under the influence of environmental shear, the middle-level and upper-level vortices of the incipient storm initially drift away from the surface center (0–24 h, Figure 3a) before the tilted vortex column begins its precession. Coincidently, the local shear vector in each composite consequently changes direction cyclonically as a result of an extrashear component caused by the vortex vertical structure

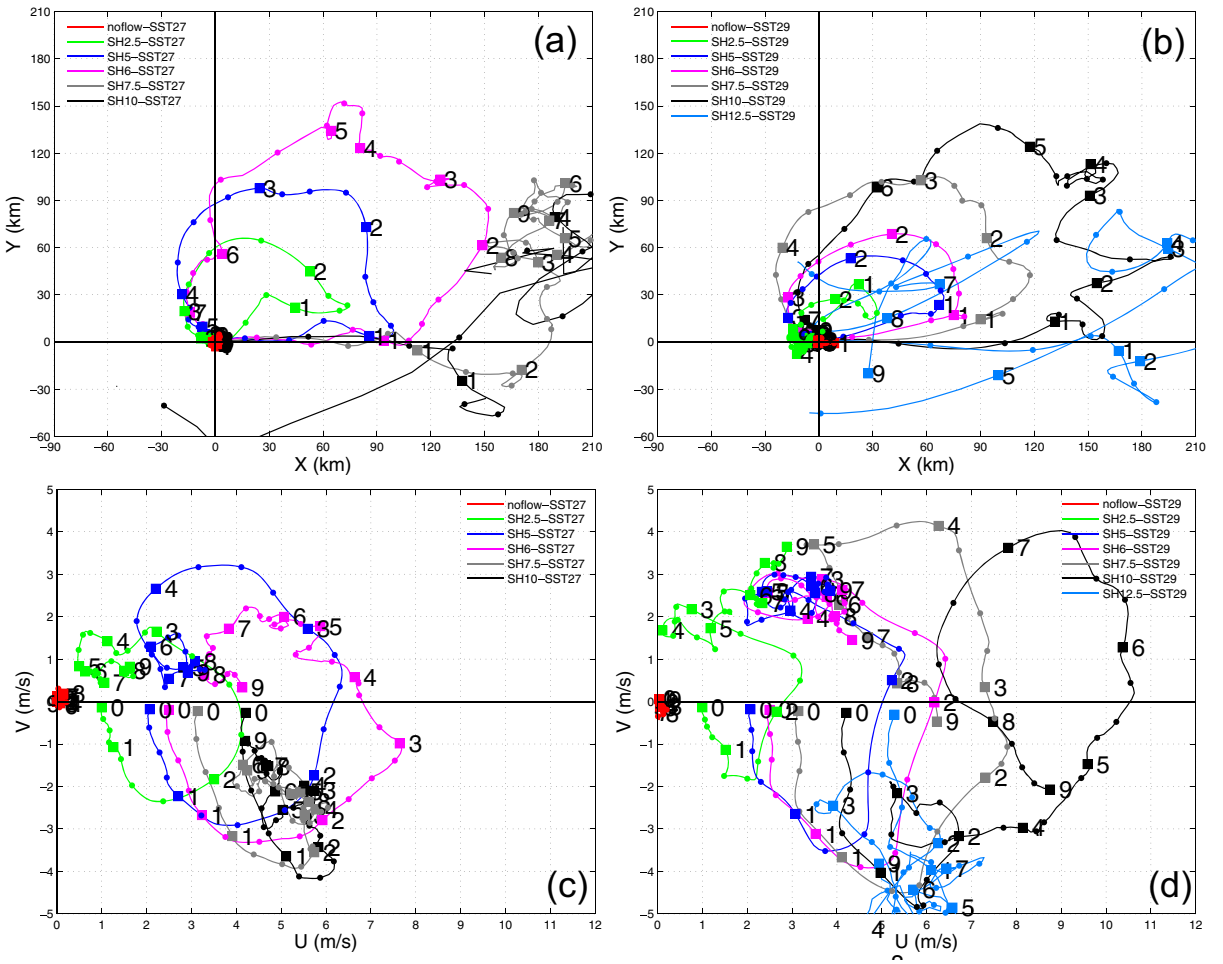

Figure 3. (a) Time evolution of tilt vectors under SST27; (b) the same as Figure 3a except for SST29; (c) time evolution of shear vectors under SST27; (d) the same as Figure 3c except for SST29. Dots are at 6 h intervals; squares are at 24 h intervals. Numbers besides the squares show the simulation time in days. Vectors all originate from (0, 0) and end on lines.

decoupling before alignment pointing to the right of the tilt vector. Under the shear conditions, besides the variation of the shear vectors, there are large deviations in the evolution of the tilt vectors that lead to subsequent differences in the timing of the RI onset. SH2.5-SST27 has the shortest and smallest precession cycle among all sheared simulations. During the first 24 h of the simulations, the tilt magnitudes of SH5-SST27, SH6-SST27, and SH7.5-SST27 increase at a comparable pace (Figure 3a), although the vortices in SH7.5-SST27 tilt slightly farther toward the downshear side before the precession starts. After the precession starts around 24 h, systematic differences appear among these three experiments with only a slight difference in the environmental vertical shear. SH5-SST27 has the smallest tilt vector with the largest tilt magnitude of about 120 km. SH6-SST27 starts precession about 12 h later than SH5-SST27 and finally completes precession and aligns after approximately 7 days, even with the largest tilt magnitude reaching 180 km. The tilt of SH7.5-SST27 continues to increase and the vortex column precesses cyclonically to about 20° before stopping at the downshear left quadrant with a tilt magnitude of up to 230 km. Further increase the vertical shear to 10 m/s for SST27 (SH10-SST27) will lead to farther downshear tilt of the vortex and eventual failed precession, as in SH7.5-SST27.

The same environmental shear conditions are utilized for the SST29 experiments that have a higher SST (29°C) than that in SST27, with the addition of an even larger shear condition of 12.5 m/s (Figures 3b and 3d). The evolutions of the developed vortices are similar to the ones that develop under the lower SST condition. When the experiments that have the same shear condition under different SSTs are compared (e.g., SH6-SST27 and SH6-SST29), we can clearly see that with higher SSTs, the precession process starts earlier and almost at the same time as the increase of the tilt magnitude. In addition, the magnitude of the tilt

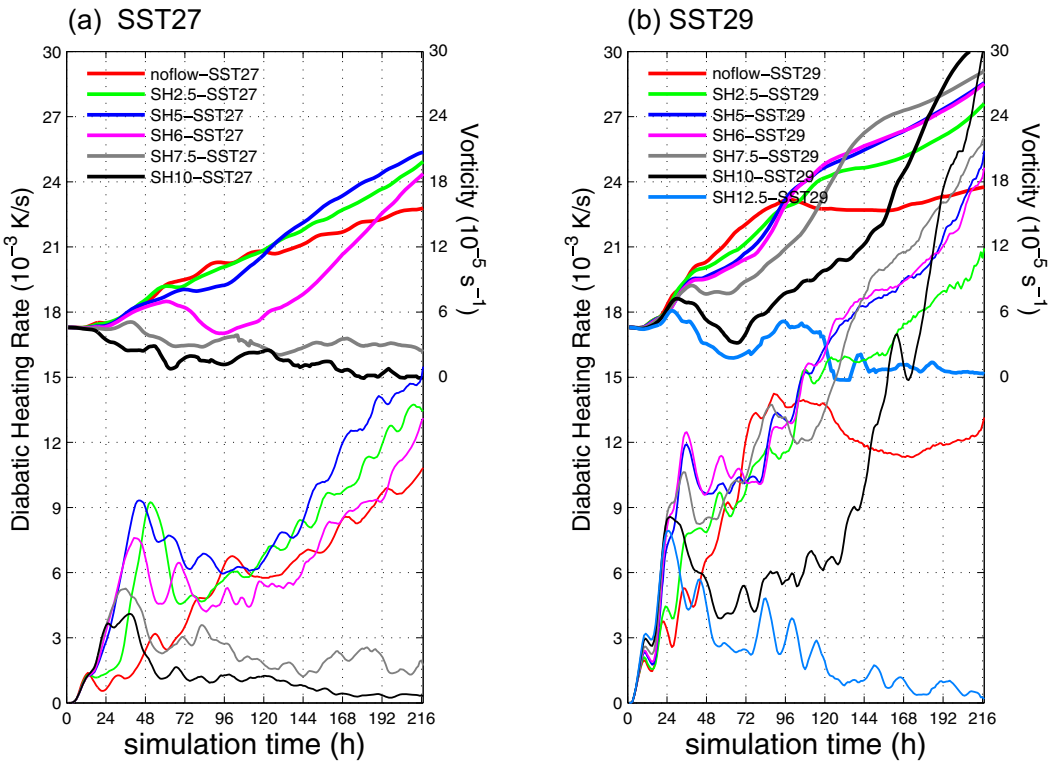

Figure 4. (a) Time evolution of 450 hPa relative vorticity (thick lines, right axis) and column-integrated diabatic heating rate (thin lines, left axis) under SST27; (b) the same as Figure 4c except for SST29.

vector of SH6-SST29 is much smaller than that of SH6-SST27. For the larger shear conditions of SH7.5 and SH10, the precession and alignment processes reach completion under SST29, both of which fail to develop under a lower SST (27°C). The possible explanation in this difference of development is owed to more diabatic heat release under higher SST, which will be discussed in section 6.

3.2. Midlevel Vorticity and Diabatic Heating Evolution

Due to the importance of convection and diabatic heating on the development of TC vortices, the evolution of the diabatic heating and vortex strength is explored. We utilize the 450 hPa average vorticity within a 250 km radius centered on the 450 hPa circulation center as the strength of the TC midlevel vortex. It is clear that the vortex intensity changes are closely related to the diabatic heating rate (Figure 4). For SST27, a continuous increase in both the midlevel vortex strength and diabatic heating rate is observed in the noflow case, which is consistent with the 10 m maximum wind speed evolution in Figure 2a. The diabatic heating rate in SH2.5 is greater than that of noflow while lower than cases with shear amplitudes 5 m/s or larger during 24 to 36 h; the diabatic heating rates of SH5, SH6, SH7.5, and SH10 are similar to each other over the first 24 h of the simulations for SST27 (Figure 4a).

However, after 24 h, larger shear magnitudes lead to an earlier decrease in the diabatic heating rate for SST27. The divergence in the diabatic heat release likely leads to differences in midlevel vortex strength, with a lag time of approximately 12 h. For example, the SH5-SST27 vortices have a temporal local maximum in diabatic heating at 44 h. After that, the magnitude of diabatic heating rate first decreases to a temporal local minimum magnitude of 6×10^{-3} K/s at 96 h and then begins to increase afterward. At the same time, the midlevel vorticity of SH5-SST27 continuously increases. In comparison, the midlevel vorticity of SH6-SST27 first decays from 60 to 96 h and then intensifies after the diabatic heating starts to increase. Meanwhile, SH7.5 and SH10 both have a much smaller diabatic heating rate and the midlevel vorticity decreases after the first burst of convection which never recovers (Figure 4a).

With a higher SST (Figure 4b), the vortices that develop have larger magnitudes of diabatic heat release and are accompanied by stronger midlevel vortices in SST29. Both the noflow and SH2.5 simulations of SST29

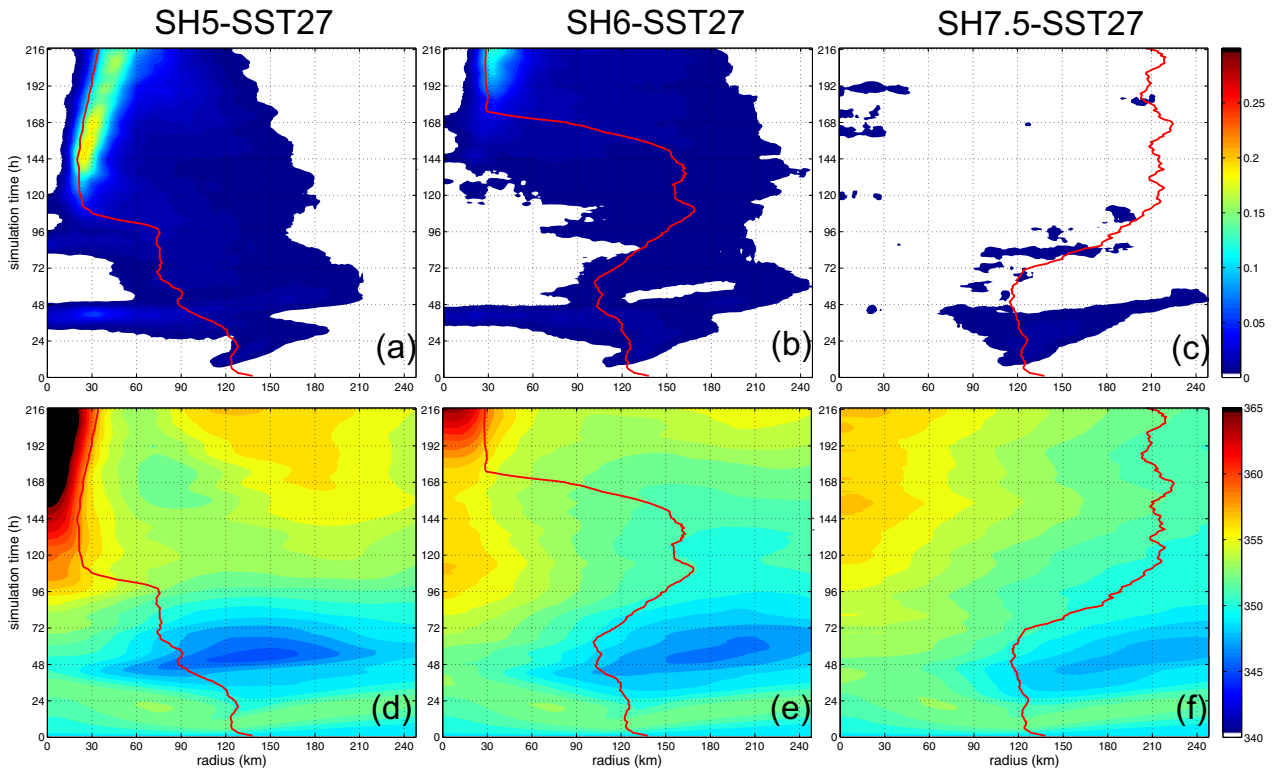

Figure 5. Time evolution of azimuthally averaged column-integrated positive-only diabatic heating rate (K/s) for (a) SH5-SST27, (b) SH6-SST27, and (c) SH7.5-SST27. Time evolution of azimuthally averaged boundary layer equivalent potential temperature (K) for (d) SH5-SST27, (e) SH6-SST27, and (f) SH7.5-SST27. Red line is the radius of maximum tangential wind (RMW).

now have a nearly continuous increase in diabatic heating rate while the temporal reduction in diabatic heating rate for moderate wind shear conditions (SH5, SH6, and SH7.5) after the initial burst of convection becomes less apparent (Figure 4b).

The only simulation with a temporal reduction in diabatic heating and later revival is SH10 for SST29. Further increase of the shear to 12.5 m/s on the other hand will have continued decrease in diabatic heating after the initial burst of convection (the storm fails to develop and the vortex fails to complete precession as in Figures 3b and 3d). There are smaller scale fluctuations in the evolution of the diabatic heating, which are believed to result from the typical life cycle of moist convection. It is also important to keep in mind that the calculation of the vortex centers of SH7.5-SST27, SH10-SST27, and SH12.5-SST29 at the later simulation times in Figure 3 is not completely reliable because the vortices are rapidly weakening (Figure 4) and the weighted vorticity centers may not be representative of true vortex centers in each experiment.

4. Convection Modification

To further understand how shear modifies convection and diabatic heating, and subsequently the vortex structure and intensity, we will primarily focus on three ensemble composites in the remainder of this paper: SH5-SST27 (blue in Figure 4a), SH6-SST27 (magenta in Figure 4a), and SH7.5-SST27 (grey in Figure 4a). These composites represent the simulations in which the vortices intensified the quickest, the vortices develop after a long time of struggle, and the vortices that failed to ever develop, respectively. When the time evolution of the azimuthal average of the vertically integrated diabatic heating rate as a function of radial distance is examined (Figures 5a and 5c), a stronger burst of convection induces expansive diabatic heating within the radius of maximum azimuthally averaged tangential wind (RMW; Figures 5a and 5b) around 36–48 h under smaller shear conditions. The location of the RMW is closely related to the location of the convection. SH5-SST27 contracts its strong convection within the radius of 120 km quickly after 48 h (Figure 5a), while the convection associated with SH6-SST27 extends to a 200 km radius (after struggling to

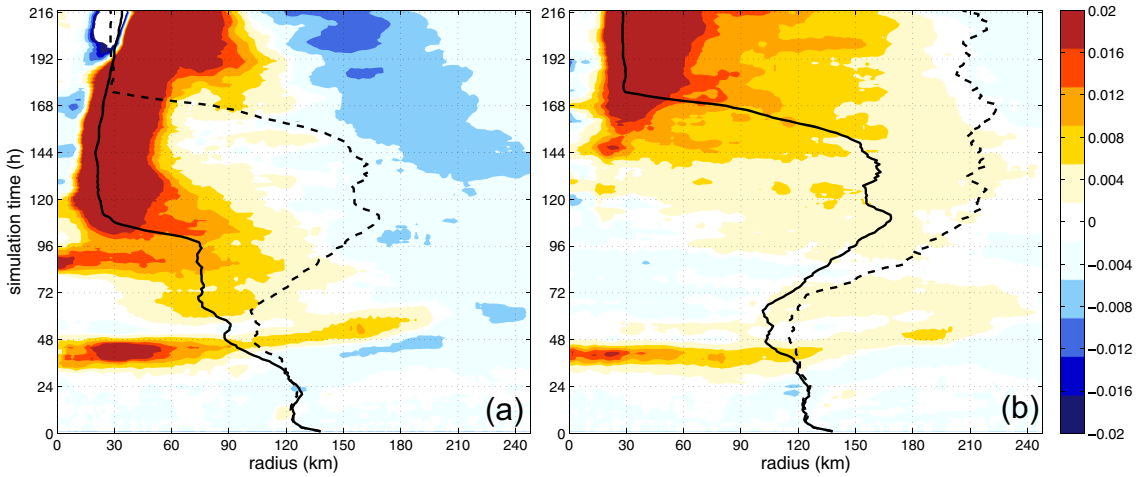

Figure 6. Time evolution of column-integrated positive-only diabatic heating rate (K/s) difference between (a) SH5-SST27 and SH6-SST27 and between (b) SH6-SST27 and SH7.5-SST27.

intensify between 60 and 144 h). SH6 eventually succeeds in contracting the area of convection, resulting in a smaller RMW (Figure 5b). SH7.5-SST27 has only weak and sparse convection after 58 h, which is not able to contract due to the lack of effective strong convection even after 120 h (Figure 5c). The plots of diabatic heating difference in Figure 6 clearly present the relative location and strength of the convection. The smaller shear case SH5-SST27 (SH6-SST27) has more diabatic heating close to the surface center and smaller RMW than SH6-SST27 (SH7.5-SST27).

The above analysis shows a clear relationship between the convective heating and the development of a TC vortex under the moderately sheared environment. As discussed in section 1, currently there are two prevailing theories about the effects of vertical wind shear on TC development: (a) the ventilation effect, which involves midlevel dry air [e.g., *Tang and Emanuel*, 2010; *Riemer et al*., 2010] and (b) the effect of vertical wind shear on the spatial distribution and intensity of convection and the feedback between convection and vortex strength [e.g., *Wang*, 2009; *Fudeyasu and Wang*, 2011]. Both hypotheses recognize the influence of shear on the TC development by modulating convection. As described in *Tang and Emanuel* [2010], the pathway of midlevel ventilation works by precipitation-induced subsidence that flushes the midlevel dry air down to the boundary layer, which subsequently reduces the equivalent potential temperature of the boundary layer air. This dry air is then advected into the updraft by radial inflow, which weakens the TC intensity as a result of less latent heat release and weaker convection. The other pathway that the reorganization of convection can impact TC intensity is through the tilting of the vortex column, which rearranges the convection to the downtilt side ("downtilt" is defined as the direction along the tilt vector direction). This new convection distribution can impact the vortex intensity and the low-level convergence, before weakening the convection itself.

In order to verify which effect is the dominant one during the formation of a sheared TC in our simulations, both mechanisms are explored in greater detail next.

4.1. The Influence of Dry Air Ventilation on TC Formation

The time evolutions of the azimuthally averaged boundary layer θe (Figures 5d–5f) show that the boundary layer θe decreases during the first burst of convection (30–54 h) for all three composites with different shears. This decrease represents the process of subsidence of the midlevel dry air. When we examine the whole period of lower θe (24–72 h), the SH7.5-SST27 experiments have a much weaker dry air ventilation when compared to SH5-SST27 and SH6-SST27. It is clear that the area of low θe air is around and outside the RMW, which is because the convection is closely associated with the maximum wind at the surface and the precipitation location corresponds to the location of low θe air at the boundary layer.

The horizontal plots of boundary layer θe in Figure 7 show that before vortex alignment happens, the inflow is mainly under the convective region as it moves cyclonically accompanying the vortex precession. The

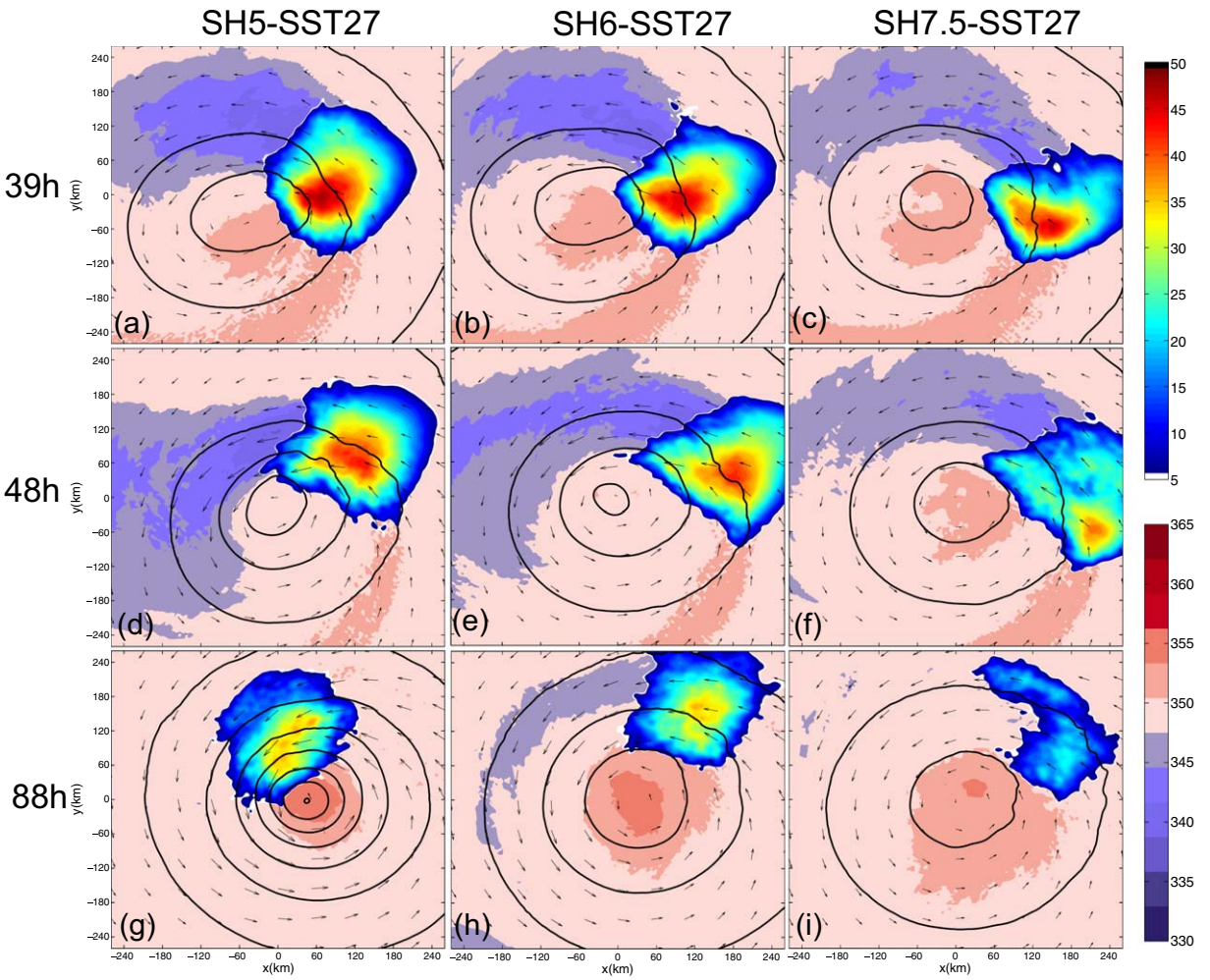

Figure 7. The 10 m surface wind vectors, mean sea level pressure, boundary layer equivalent potential temperature (average between heights of 250 m, 500 m, 750 m, and 1 km; K, pink and purple colorbar) and column-maximum reflectivity (dBZ, red and blue colorbar) at 39, 48, and 88 h. (left column) SH5-SST27, (middle column) SH6-SST27, and (right column) SH7.5-SST27.

low θe air is located under and downstream of the convection cluster. This occurs due to the advection of the low θe air by the vortex mean flow in addition to moving radially outward. This radial advection of the low θe air also can be seen in Figures 5d–5f, as the areas of low θe air extend to large radii with time. If we trace the dry air evolution forward in time (Figure 7, columns), we find that the dry air can be recovered by the sea-surface flux (per wind-induced surface hear exchange or WISHE mechanism of *Emanuel* [1986]) before it is able to reach the updraft that is located upstream of the vortex mean flow.

The value of boundary layer θe is related to the convection strength, which is controlled by the environment shear conditions. Stronger convection produces stronger downdrafts, and therefore more dry air is flushed into the boundary layer. Because of weaker convection in SH7.5-SST27 (Figures 7c, 7f, and 7i), the amount of dry air flushed down to the boundary layer is much less than that in SH5-SST27 (Figures 7a, 7d, and 7g) and SH6-SST27 (Figures 7b, 7e, and 7h). The ventilation effect through boundary layer inflow is not clear when the vortex is weak in part because there is no sufficient radial inflow to advect the low θe air into the updrafts. Meanwhile, the low θe air from the midlevels, which can be seen from the θe contour in Figure 12, is also able to recover before reaching the updraft location due to the fact that the updrafts are mainly upstream of the low θe air, and the distance that this low θe air has to travel is sufficiently long to allow for the completion of the recovery process, as part of the WISHE process. This indicates that the dryness of the midlevel air may influence the formation of the tropical cyclone depending on the relative location of the updraft and the dry air.

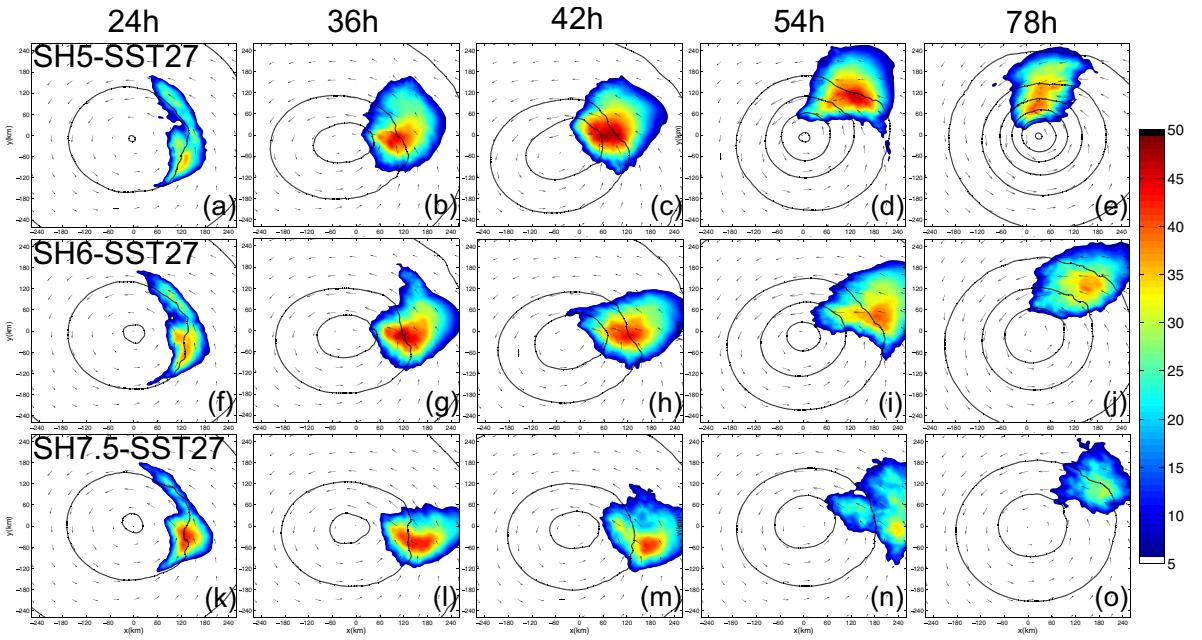

Figure 8. Sea level pressure (contour), surface wind (vector), and maximum reflectivity (shading) at 24, 36, 42, 54, and 78 h. (top row) SH5-SST27, (middle row) SH6-SST27, and (bottom row) SH7.5-SST27.

4.2. Effect of Vertical Wind Shear on the Spatial Distribution and Intensity of Convection and the Feedback Between Convection and Vortex Intensity

In all sheared simulations, deep convection starts to develop due to enhanced convergence induced at the downtilt direction of the vortex (Figure 8) [*Zhang and Tao*, 2013, Figure 5]. This downtilt wave number-one positive vorticity anomaly can be enhanced by the diabatic heating from deep convection. The TC vortex precession process results from the cyclonic advection of the upper-level vorticity anomalies by the primary

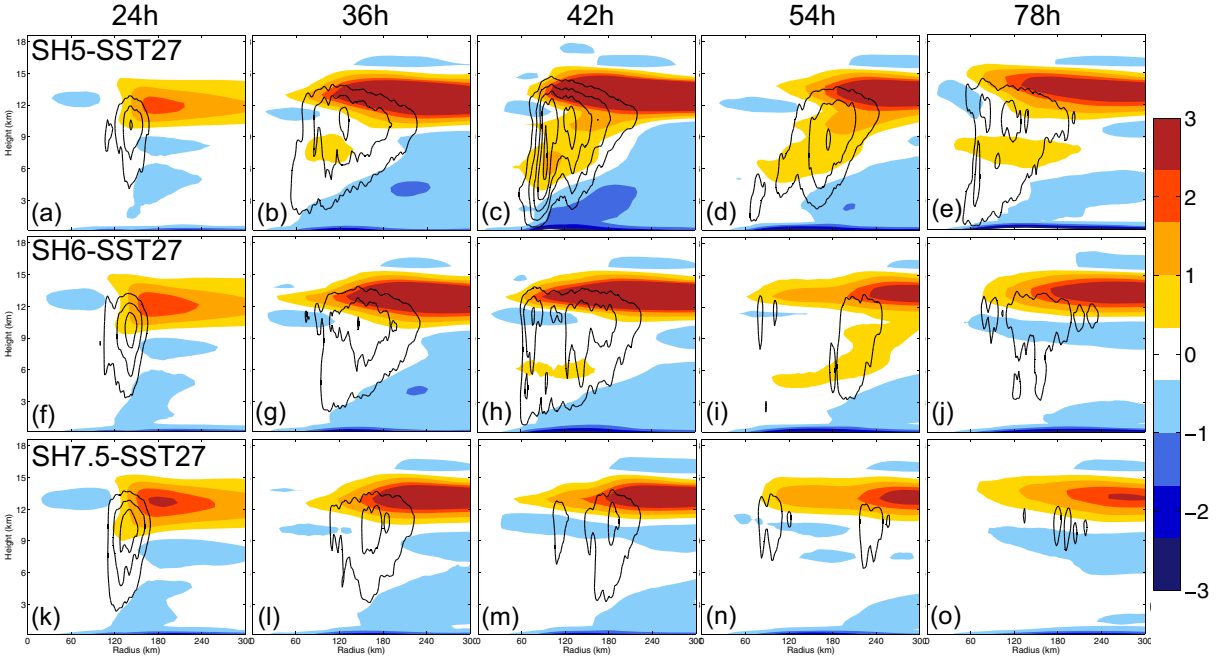

Figure 9. The azimuthally averaged vertical wind (contour) and radial wind (m/s, shading) at 24, 36, 42, 54, and 78 h. (top row) SH5-SST27, (middle row) SH6-SST27, and (bottom row) SH7.5-SST27.

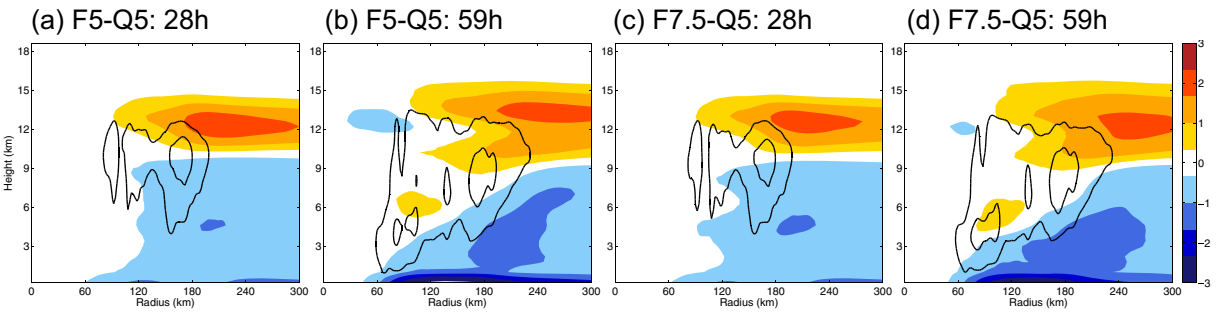

Figure 10. The azimuthally averaged vertical wind (contour) and radial wind (shading) of the Sawyer Eliassen Equation output. The heating and background forcing are separated. (a and b) Using SH5-SST27 heating and background forcing; (c and d) using SH5-SST27 heating and SH7.5-SST27 background forcing.

(mean) vortex circulation (Figures 3a and 3b), which is also shown as the cyclonic movement of the convection cluster and the anticlockwise rotation of the tilt vector (Figure 8). Due to the influence of the larger radial outward component and tangential backward component of the environmental wind on the middle-level and high-level vortices in the downshear left quadrant, the vortex column becomes more slantwise as it starts to precess. The larger tilt slows the vortex precession speed (Figures 3a and 3b) since the upper-level vortex anomalies will be advected by weaker mean tangential wind from the primary vortex. However, the tilt magnitude begins to decrease (and the precession speeds up) when the tilt vector reaches around 30–45° to the north of the environmental shear vector by which time the effective shear projecting on the tilting direction is considerably reduced.

After the tilt vector precesses past 90° to the north of the environmental shear vector, a dramatic decrease of the tilt magnitude occurs by which time the westerly environmental shear begins to pushes the convection (and the upper-level vortex) closer to the surface center and straightens the vortex column. The most important factor dictating the completion of precession is the changing of the tilt vector from the downshear to the upshear side (Figure 3); the vortices with tilt vectors that cannot turn over the 90° to the north of the environmental shear vector fail to develop (SH7.5-SST27, SH10-SST27, SH12.5-SST29) (Figures 2 and 3). For the vortices that do subsequently develop into TCs, the divergence of the evolution of tilt vectors begins with differences in precession, which have a large dependence on the vortex strength. Since convection is critical to support the vortex strength (Figure 4), it is of great importance to examine the evolution of convection and resultant diabatic heating under different shear conditions.

Section 3.2 (Figure 6) has shown that stronger diabatic heating rates are closer to the primary vortex surface center under smaller shear conditions (SH5-SST27) than under larger shear (SH6-SST27) conditions, and the diabatic heating rates are weaker for nondeveloping TCs (SH7.5-SST27). In order to obtain an improved understanding of the evolution of the convection and TC strength during precession for the three composites, we further examined the horizontal plots of radar reflectivity, sea level pressure, and 10 m wind shown in Figure 8. This set of figures demonstrates the strong divergence of the convection structures and TC intensities among different shear conditions during the periods of vortex tilt and precession. This reinforces the effect of vertical wind shear on the formation of TCs under different magnitudes of environmental shear, despite only a small difference (1–2 m/s) in shear magnitude. Note that the reflectivity strength of SH5-SST27 at 24 h is weaker than that of SH6-SST27 and SH7.5-SST27 (Figures 8a, 8f, and 8k), the cause of which will be discussed further in section 5. At 36, 42, and 54 h (Figures 8l–8n), the convection associated with SH7.5-SST27 undergoes a dramatic decrease in strength and begins to drift radially outward. While the tilt vector of SH5-SST27 successfully precesses over the downshear left quadrant to the upshear left quadrant (Figure 8e), the convection cluster of SH6-SST27 strengthens and weakens several times (not shown) and precesses at a much slower speed. Meanwhile, convection of SH7.5-SST27 continues weakening and is advected farther away from the surface center with little precession of the tilt vector (Figures 8n and 8o). The sea level pressure contours in Figure 8 also highlight the differences in the strength of the vortices under the varying environmental wind shear conditions.

Consistent with Figure 8, azimuthally averaged radial and vertical winds are plotted at different times in Figure 9. At 24 h, there are very few differences among the composites, although SH6-SST27 and SH7.5-SST27

have slightly stronger vertical wind and outflow than SH5-SST27 (since stronger shear initially induced stronger convection; see section 5). At later hours of the simulations (36 h, 42 h), SH5-SST27 develops stronger convection much closer to the surface center (Figures 9b and 9c), while the corresponding tilt slightly decreases (Figure 3a). From 42 to 54 h (Figures 9c and 9d), the main convection cluster drifts away, which is consistent with the increasing tilt magnitude in Figure 3a. Though at 54 h, the convection is far away from surface center, there is a developing updraft at a radius of approximately 60 km that subsequently merges with the primary convection cluster at later times (not shown). This supply of inner-core convection is very important to resist a larger tilt magnitude (Figure 9e), which is consistent with the finding in *Frank and Ritchie* [2001]. When analyzing the outflow of SH6-SST27 and SH7.5-SST27 in Figure 9, it is apparent that the outflow region of SH6-SST27 is farther away from the surface center at 54 h compared to SH5-SST27, while the outflow of SH7.5-SST27 is even farther. From the above analysis of the secondary circulation, it is quite clear that when the convection drifts away from the primary TC surface center, it becomes weaker and the corresponding secondary circulation is also weakened.

We have shown that the intensity and distance to the surface center of the moist convection has a strong relationship with the TC's secondary circulation (Figure 9), while horizontal cross sections of the vortices (Figure 8) allowed us to illustrate the relationship between vortex strength and convection. In summary, the vertically displaced vortex column of the developing TCs (SH5-SST27 and SH6-SST27) leads to the downtilt of the convective cluster (and associated upper-level vortex anomaly), which first is advected away from the surface center by the shear. Advection of the upper-level vortex anomaly by the primary vortex subsequently leads to the precession of the tilt vector. The closer the convective cluster to the primary vortex, the stronger the secondary circulation and the more efficient the convection is to enhance the primary vortex which in turn could lead to more expedited precession. When the shear is large (SH7.5-SST27), the convective cluster (and the upper-level vortex anomaly) will be advected to a farther radial distance, and the convection and secondary circulation strength are comparatively weaker. Consequently, the precession process fails to complete, which leads to the eventual failure of the vortex alignment and the TC struggles to develop.

4.3. Background Circulation and Heating Impacts on the Secondary Circulation

In section 4.2, we have illustrated the relationships between changes in convection, the main circulation and the secondary circulation of a potentially developing vortex. Since vortex strengthening results from the advection of vorticity inward to the core of the vortex by the secondary circulation, we will next investigate the relative importance of the main circulation of the vortex (treated as background circulation) and convective diabatic heating on the strength of the secondary circulation.

We introduce the Sawyer-Eliassen (SE) Equation [*Eliassen*, 1951] to quantitatively evaluate the contribution of the background circulation and the diabatic heat forcing on the secondary circulation. The SE model used here is following *Montgomery et al*. [2006], *Fang and Zhang* [2011], *Rozoff et al*. [2012], and *Sun et al*. [2013]. A detailed description of the SE equation can be found in the Appendix of *Sun et al*. [2013]. The momentum forcing (F) and the heat forcing (Q) can be separated. We change the momentum forcing in SH5-SST27 to the momentum forcing from SH7.5-SST27 and keep the heat forcing. The two SE outputs are denoted as F5-Q5 and F7.5-Q5.

The forced secondary circulation that results (Figures 10c and 10d) after replacing the background circulation of SH5-SST27 with that of SH7.5-SST27 is almost the same as the original secondary circulation (Figures 10a and 10b). The structures of the vertical motion and radial flow are similar. The strength of the radial flow is only slightly weaker under the SH7.5-SST27 background flow. This result shows that the heat forcing is the dominant factor in driving the secondary circulation since the replacement of the background flow does not change the strength of the updrafts or the radial flow significantly. Hence, in the SH7.5-SST27 case, the convection that is weaker and farther from the surface center than in the smaller shear cases leads to a weak secondary circulation and a vortex that is unable to intensify.

Therefore, a larger tilt magnitude leads to a weaker vortex (Figures 3a, 3c, and 4), and the diabatic heating (Figure 4) that drives the secondary circulation is much weaker. The vortex strength will subsequently be even weaker, and the precession of the tilt vector will be slow and difficult, which is described in section 4. With a weakening vortex, convection weakens. A larger shear disrupts the preferred cycle of the convection-vortex feedback.

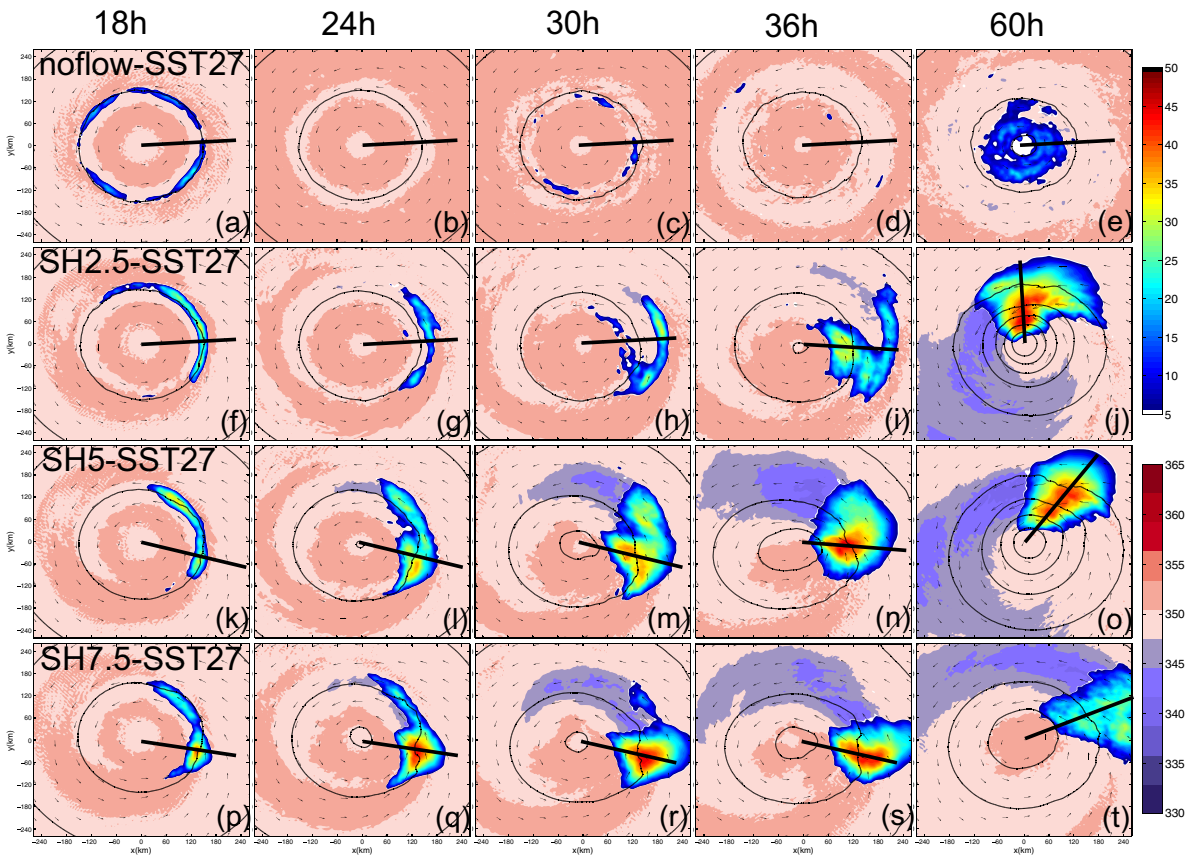

Figure 11. The 10 m surface wind vectors, mean sea level pressure, boundary layer equivalent potential temperature (average between heights of 250 m, 500 m, 750 m, and 1 km; pink and purple colorbar) and column-maximum reflectivity (dBZ, red and blue colorbar) at 18, 24, 30, 36, and 60 h. (row 1) noflow-SST27, (row 2) SH2.5-SST27, (row 3) SH5-SST27 and (row 4) for SH7.5-SST27. The thick black line is the place of the cross section in Figure 12.

5. The Beginning of the 10 m Wind Increase

As previously observed above (Figures 2c–2d), an increase in the 10 m wind for sheared TCs in the early stages of the simulations occurs. To examine this phenomenon further, Figures 2e and 2f depict the 10 m winds for the first 72 h of the simulations. The 10 m winds of the noflow case do not increase significantly before the onset of rapid intensification. However, while under various shear conditions, the 10 m winds begin to diverge at 15 h. In addition, the larger the shear magnitude, the earlier the initial wind increase starts. Since the maximum wind is associated with the convection and vortex strength, first we check the horizontal plots (Figure 11) of maximum reflectivity, sea level pressure, and boundary layer θe of four typical shear conditions (noflow-SST27, SH2.5-SST27, SH5-SST27, and SH7.5-SST27). At 18 h, SH7.5-SST27 has larger and stronger convection locating at downshear side while noflow-SST27 has weak nearly axisymmetric convection within RMW. At two later times 24 and 30 h, the convection strength is still positively related to the shear magnitude. At 36 h, SH5-SST27 catches up with SH7.5-SST27 while SH2.5-SST27 is still much weaker. But another 24 h later, it is the SH2.5-SST27 leading the convection and precession. Now the convection of SH7.5-SST27 is nearly dying while noflow-SST27 gradually organizes and intensifies its convection.

The shear here, however, has a very positive effect on the beginning 30 h of the initial convection burst. In order to understand more about how this happens, we plot diabatic heating, θe and secondary circulation in Figure 12. Each plot is the cross section of the dark black line in Figure 11, which is subjectively chosen according to the strong convection location. At 18 h, SH7.5-SST27 has presented a clear view of vertical motion. This upward motion is further enhanced at 24 h and 30 h, while SH5-SST27 develops upward motion slightly weaker than SH7.5-SST27. Both of them have some diabatic heating release. At 36 h, SH2.5-SST27 case shows clear sign of vertical motion and some diabatic heating, meanwhile the secondary

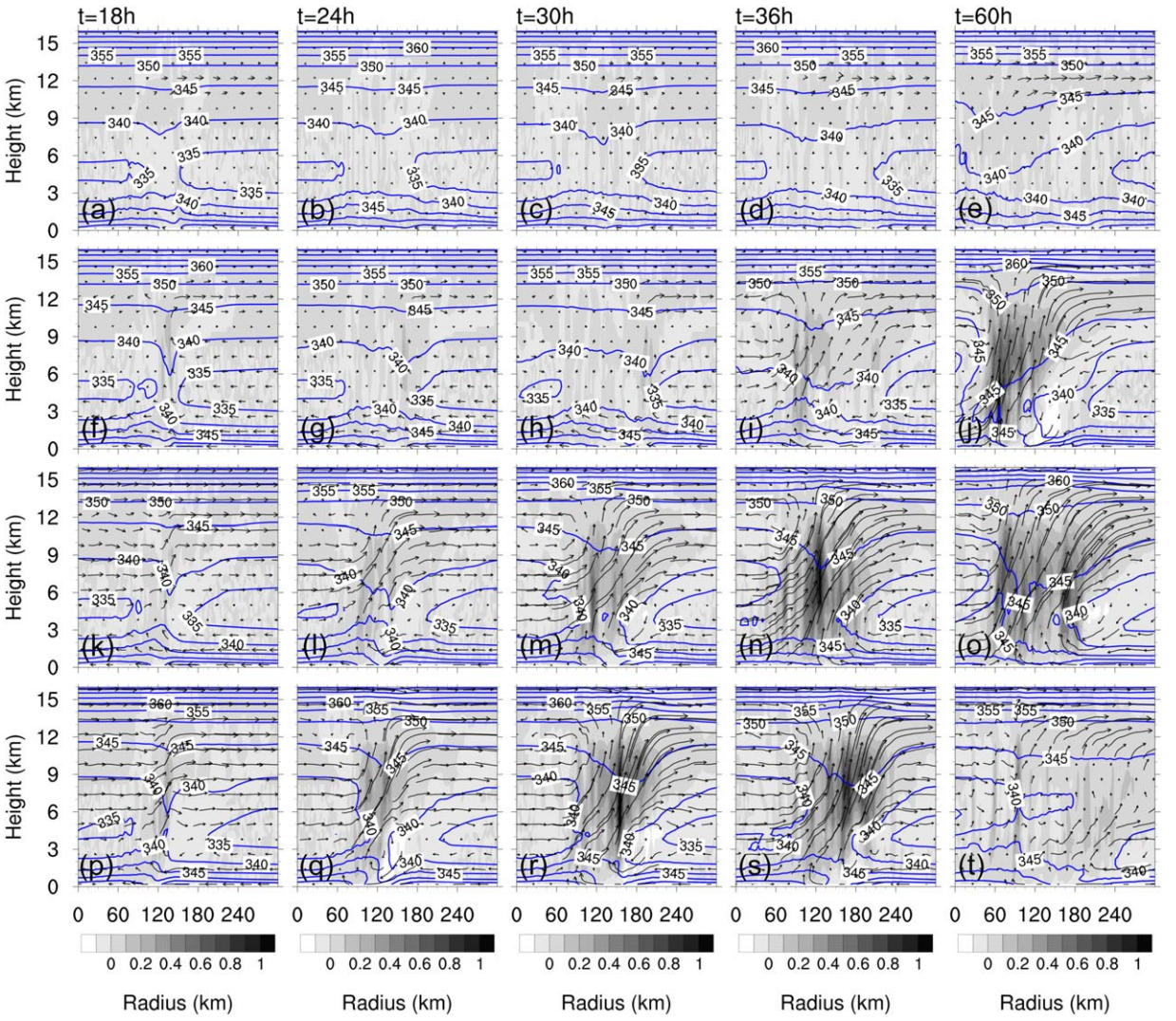

Figure 12. The cross section of lines in Figure 11 at corresponding times: blue contour for θe, curly vector for secondary circulation, and shading for diabatic heating rate (10^{-2} K/s).

circulations of SH5-SST27 and SH7.5-SST27 are much stronger and the location of SH7.5-SST27 diabatic heating is radially farther than that of SH5-SST27. At 60 h, it is clear that the secondary circulation of SH7.5-SST27 is mostly destroyed. We can see that the secondary circulation of noflow-SST27 develops slowly but steadily, while SH7.5-SST27 has much stronger upward motion at the very beginning times which initiates diabatic heating in very short time. However, this effect is temporary as the advection of midlevel and upper-level vortices by the vertical wind shear is more detrimental to the vortex strength and convection. After the weakening of the updrafts due to this negative influence of shear on convection and vortex intensity, this positive shear-to-upward motion feedback is disrupted by the shear (Figures 12p–12t).

The mechanism of shear-induced vertical motion is already explored in the previous studies [*Jones*, 1995, Figure 4]. The vertical motion anomaly is a result of forcing to achieve balanced potential-temperature perturbation after the vertical wind shear advecting the midlevel and upper-level vortices to the downshear side. It is found that the initial "dry" (no convection) vortex can benefit from the shear-induced downshear-tilt updraft anomaly to initiate convection (earlier). In the studies of a mature TC under the vertical wind shear [*Jones*, 1995, 2004; *Braun and Wu*, 2007; *Xu and Wang*, 2013], the positive anomaly can strengthen the downshear updraft and negative anomaly can weaken the upshear updraft. Furthermore, the larger shear triggers larger anomalies. In our case, since the TC initially has no convection or very weak convection, the

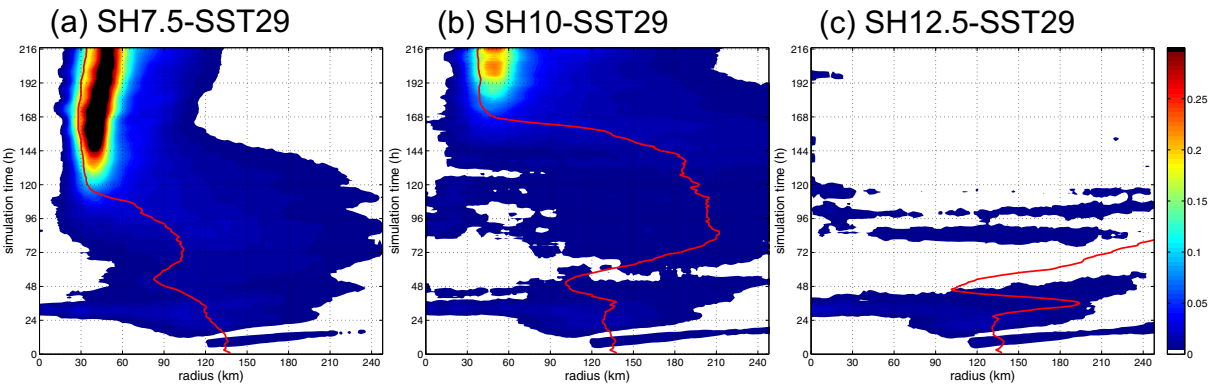

Figure 13. Time evolution of azimuthally averaged column-integrated positive-only diabatic heating rate (K/s) for (a) SH7.5-SST29, (b) SH10-SST29, and (c) SH12.5-SST29.

upward anomaly at the downshear direction helps to activate convection of which the strength is depending on the updraft strength. The updraft under higher shear is larger unless the shear is too big to maintain the balanced secondary circulation at the beginning.

6. SST Influence

As first identified in section 3.1, under higher SST conditions, vortices can resist larger shear magnitudes due to increases in the diabatic heat release. This is further demonstrated in Figure 4b, the sharp increase in the diabatic heating rate and the subsequent rapid increase in the 450 hPa relative vorticity for the sheared composites under SST29. If we compare the same shear magnitude composites under different SST, the differences are even clearer. For example, SH5-SST29 has a much smaller radius of precession for the tilt vector than

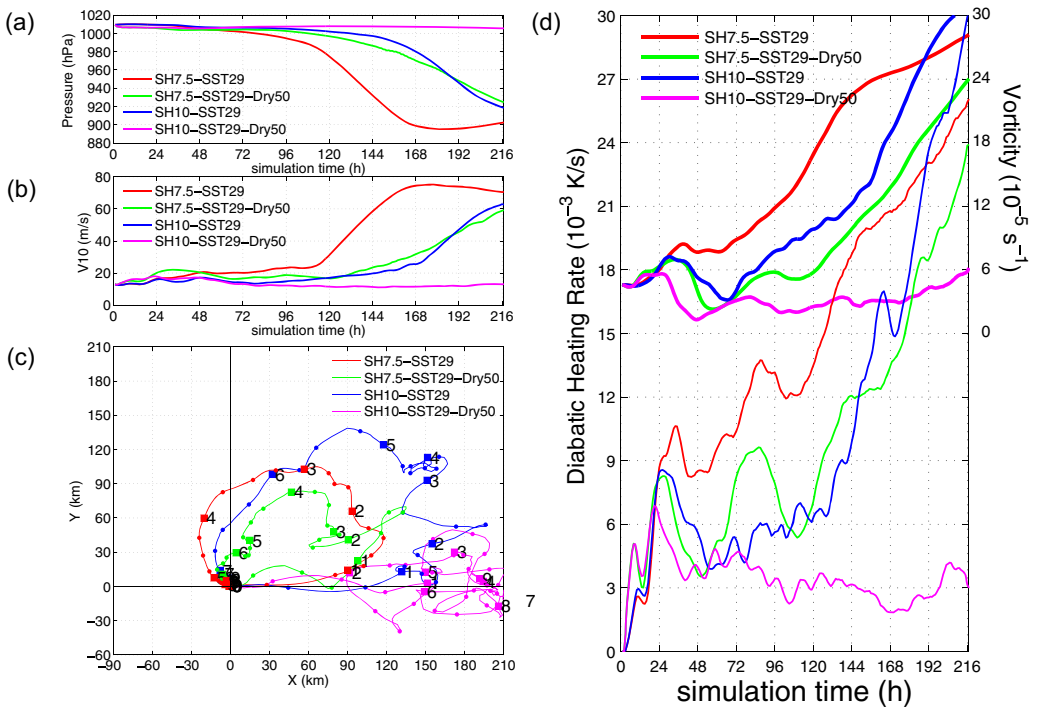

Figure 14. (a) Time evolution of minimum sea level pressure; (b) time evolution of maximum 10 m total wind; (c) time evolution of tilt vectors; (d) time evolution of 450 hPa relative vorticity (thick lines, right axis) and column-integrated diabatic heating rate (thin lines, left axis).

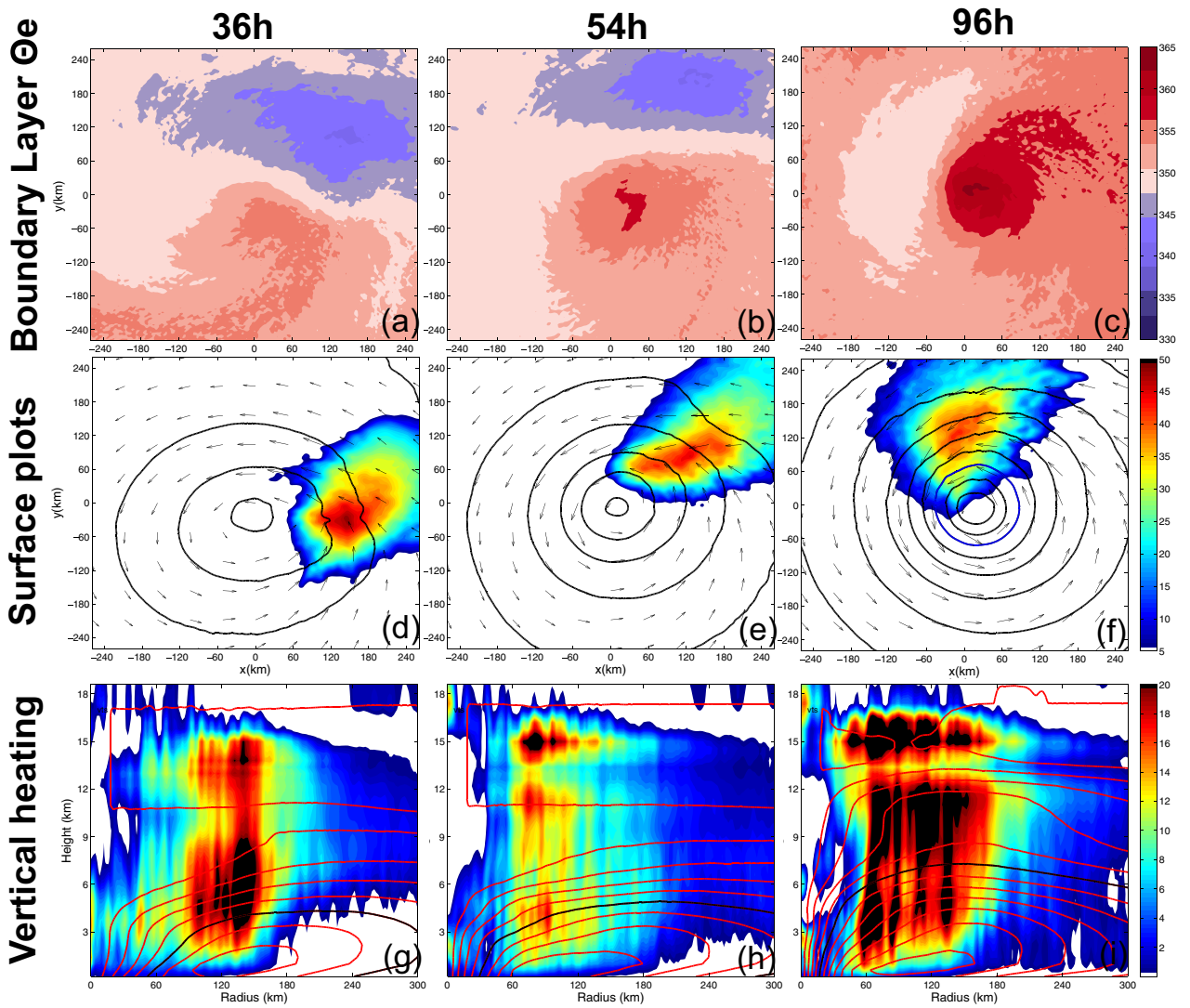

Figure 15. Plots for SH7.5-SST29. (a–c) Boundary Layer θe; (d–f) surface wind, maximum column reflectivity and sea level pressure; (g–i) azimuthally averaged diabatic heating (shading) and tangential wind (black line for 10 m/s, 2 m/s interval).

SH5-SST27, and is more comparable to SH2.5-SST27. The tilt vector associated with SH5-SST29 also begins precession immediately after it tilts. This much earlier beginning of precession results from the sharp increase of diabatic heating in SH5-SST29 and the corresponding early increase in the vortex strength (Figure 4b).

Since the importance of the convection intensity and distribution has been shown in section 4.2, the horizontal distribution and time evolution of the diabatic heating rate under SH7.5-SST29, SH10-SST29, and SH12.5-SST29 are plotted (Figure 13). It is observed that the RMW contraction timings of SH7.5-SST29, SH10-SST29, and SH12.5-SST29 are similar to that of SH5-SST27, SH6-SST27 and SH7.5-SST27, respectively. Another interesting observation is that the evolution of the tilt vectors (Figure 3a, blue line and Figure 3b, gray line) for SH5-SST27 and SH7.5-SST29 are comparable. When we compare Figures 13a–13c to Figures 5a–5c, we observe that the convection is more extensive under the higher SST condition and the amount of diabatic heating is also much greater (Figure 4a, blue line and Figure 4b, gray line). This is a possible explanation for the ability of a developing vortex to overcome higher shear magnitudes under higher SSTs. Stronger convection that results from the influence of higher SSTs leads to a faster intensification of the vortex and a smaller tilt magnitude, and this higher SST produces an increase in the critical shear value from ~6 to ~10 m/s.

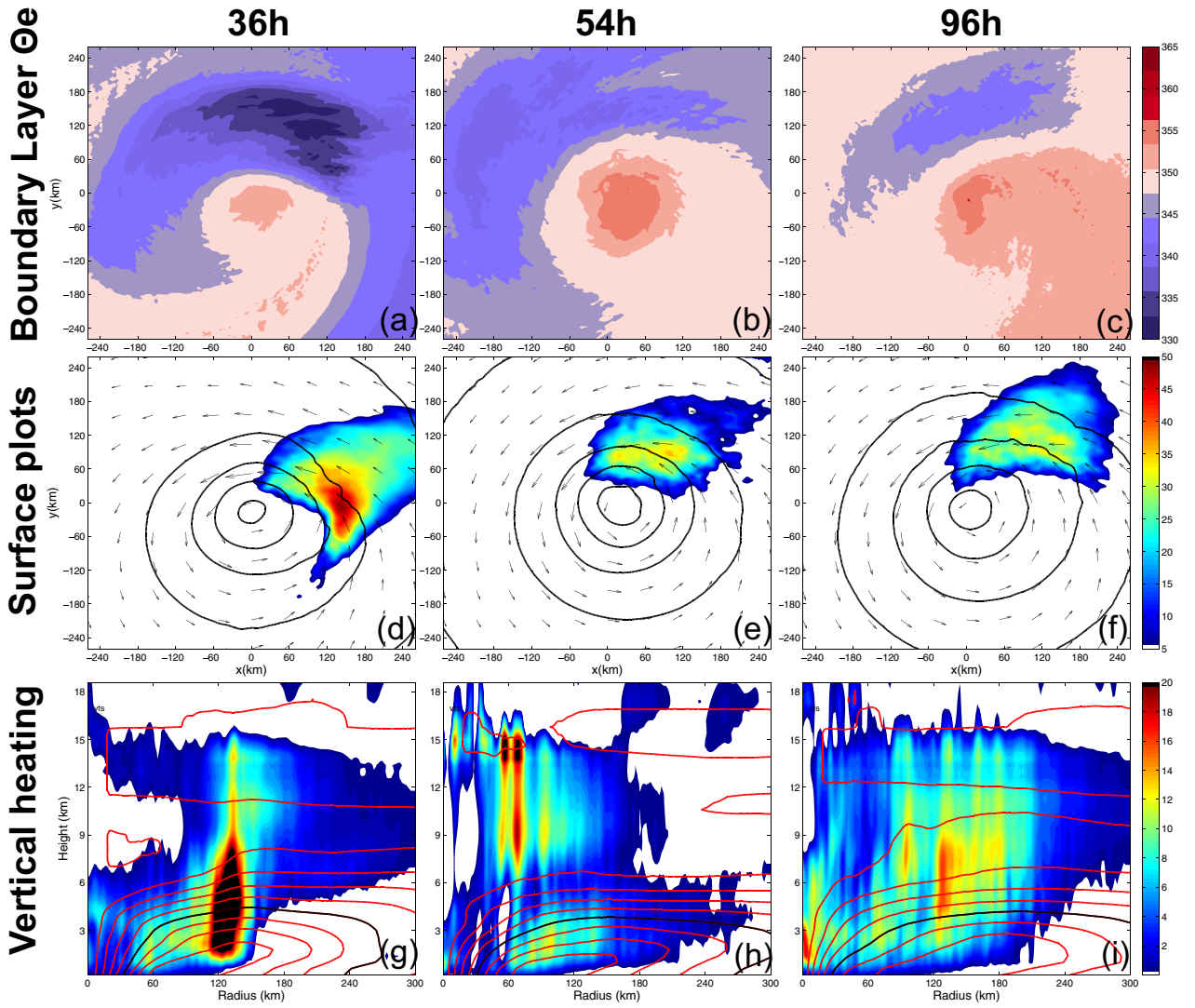

Figure 16. The same as Figure 16 except for SH7.5-SST29-Dry50.

7. Influence of Ambient Moisture Content

In section 4.1, it was demonstrated that midlevel dry air ventilation is not the dominant factor in preventing the formation of a tropical cyclone because the vortex inflow is not strong enough to advect the dry air into the updraft before the sea-surface flux recovers its moisture. Therefore, we further investigate the effect of dry air by performing additional simulations in which the environmental moisture (mixing ratio in simulation's initial condition) is reduced to 50% of its original value in all the aforementioned experiments. Figure 14 is a comparison between the moist and drier experiments of SH7.5-SST29 and SH10-SST29. It is clear that both moist experiments undergo RI after precession and alignment, while SH7.5-SST29-Dry50 needs a much longer time before undergoing RI while the drier environment experiment SH10-SST29-Dry50 weakens and fails to develop entirely.

It is interesting to note that the tilt magnitude of SH7.5-SST29-Dry50 is comparable or even smaller than that of SH7.5-SST29 (Figure 14c), however, the time for precession and alignment is about 2 days longer. For the drier environment runs, the area averaged midlevel vorticity and column-integrated diabatic heating (Figure 14d) are slightly stronger during the first 22 h and this effect on sea level pressure lasts for much longer time that even at 36 h, the dry runs have lower minimum sea-level pressure (SLP) (Figure 16). However, after 24 h, the drier environment experiments have much weaker diabatic heating and a weaker

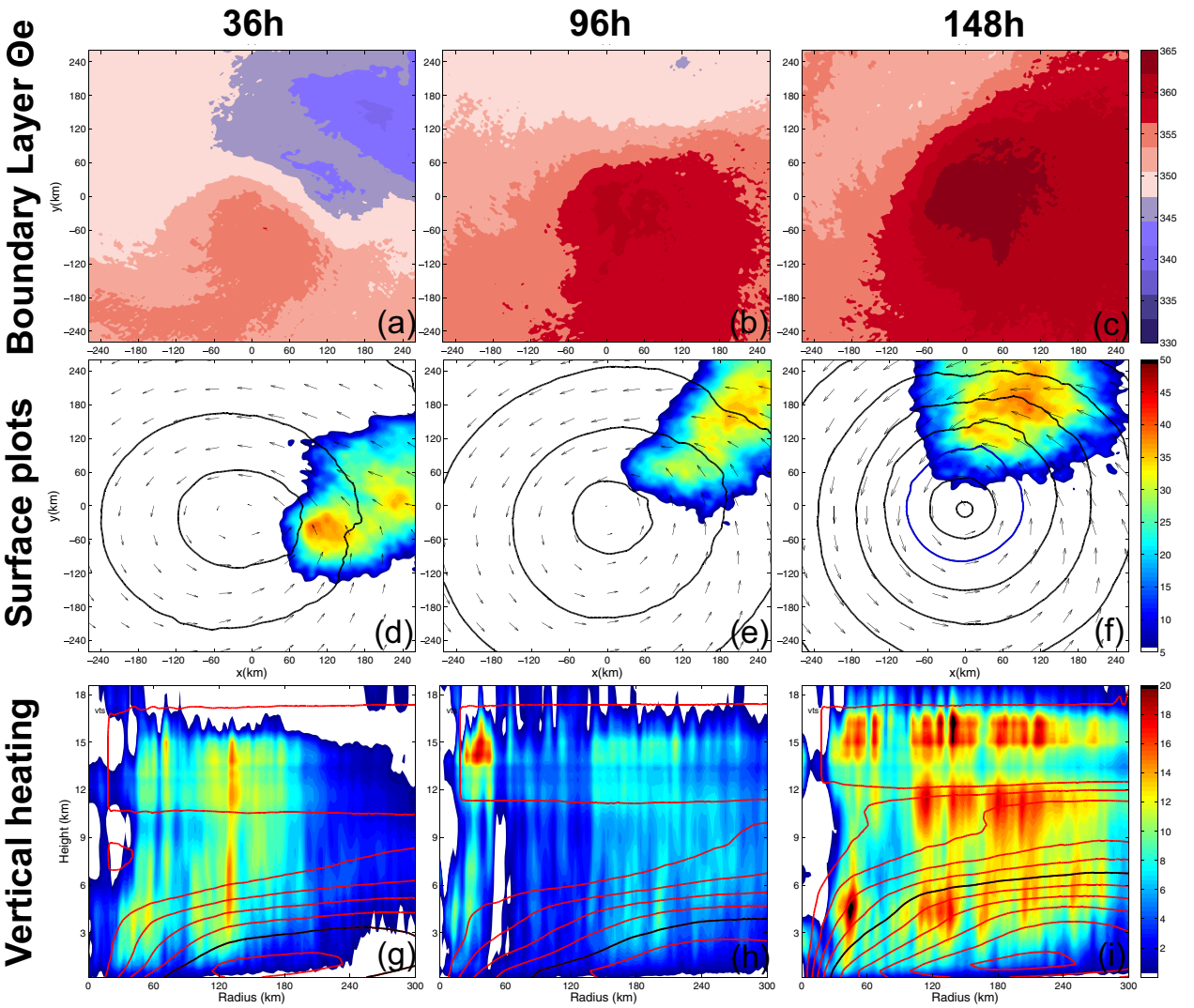

Figure 17. The same as Figure 16 except for SH10-SST29.

midlevel vortex. In the SH7.5-SST29 experiment (Figures 15e and 15f), the convection cluster extends to more than 250 km with the strongest convection close to the center, while in the SH7.5-SST29-Dry50 experiments (Figures 16e and 16f), the convection cannot develop far from the surface center and the maximum reflectivity is much weaker. This can also be seen in the radius-height plots, where the diabatic heating reaches heights of ∼17 km in the moister environment (Figures 15h and 15i), while in the drier environment, the heating cannot penetrate heights of 15 km (Figures 16h and 16i). The explanation for the dry air effects demonstrated herein is that the drier environment prohibits the development of convection far from the surface center, which confines the convection cluster within a smaller radius. Therefore, the tilt magnitude remains small throughout precession. Meanwhile, the environmental drier air weakens the convective diabatic heating, which also weakens the secondary circulation. This weakening also causes the mean circulation of the vortex to weaken, which in turn slows down the precession speed.

When we compare SH10-SST29 and SH10-SST29-Dry50 (Figures 17 and 18), it is similar to the difference between SH7.5-SST29 and SH7.5-SST29-Dry50 except that the convection in SH10-SST29-Dry50 dies. The reason for this is also the dry air diluting the convection and the feedback between the convection and the vortex strength is destroyed that the vortex is not able to resist the drifting effect of the vertical wind shear.

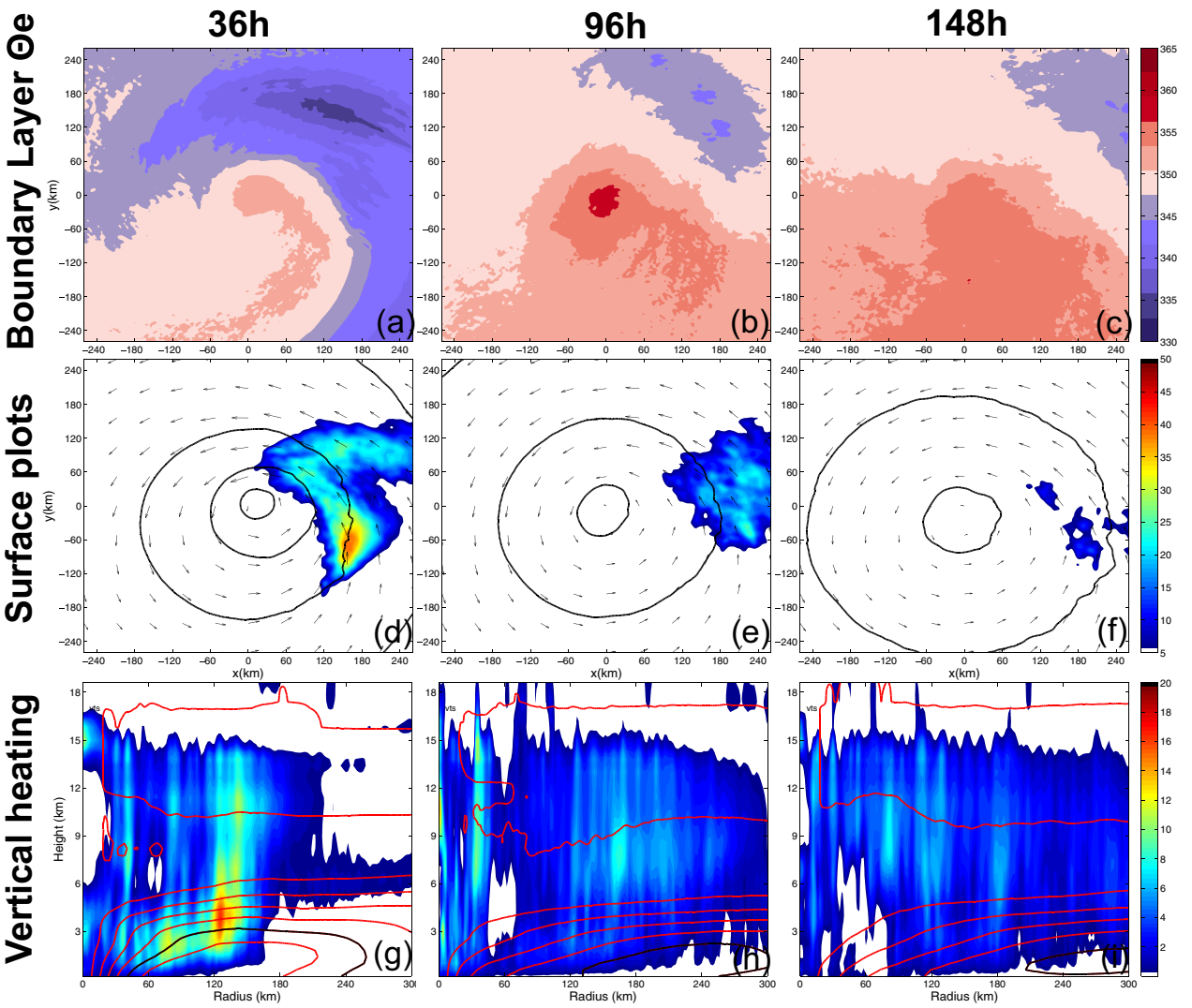

Figure 18. The same as Figure 16 except for SH10-SST29-Dry50.

It is worth noting that we reduce the whole layer moisture of the environment all around the vortex. The consequence is the dry air which is already in the environment boundary layer can be advected into the updraft region and making effect. This is different from the dry air studies done by *Ge et al.* [2013] and *Braun et al.* [2012] in which they reduced the 850–650/850–600 hPa layer relative humidity (RH) to 25%. In other words, the drier experiment conducted in this section is not specific to effect of the midlevel dry air though to a broad extent our findings are consistent with the midlevel dry air ventilation hypothesis in previous studies.

8. Concluding Remarks

This study explores the effect of vertical wind shear on the formation of tropical cyclones through composites of cloud-resolving ensemble simulations performed using the WRF model. It is found that the structure and intensity of tropical cyclones can be significantly affected by the environmental vertical wind shear. Larger environmental vertical wind shears lead to longer time before the onset of rapid intensification, primarily because of the difference in the timing of the precession and alignment processes. Upscale divergence of TCs under different shear conditions grow from discrepancies in moist convection. These differences are first observed in changes in the tilt of the incipient vortices and then in the timing of precession. Both the vertical tilt of the storm and the effective (local) vertical wind shear vectors rotate cyclonically

around the surface center with varying speeds. The tropical cyclone begins to intensify immediately after the vortex aligns, however, when the shear magnitude exceeds 7.5 m/s, the tropical cyclone may never complete the precession process unless the constant SST is increased from 27 to 29°C. In other words, the development of a tropical cyclone is largely dependent on the magnitude of vertical wind shear, but can be further affected by other environmental conditions such as sea-surface temperature and environmental dry air. Given the same magnitude of vertical wind shear, the higher SST condition produces smaller magnitude tilt vectors and therefore shorter RI onset times. In addition, the critical value of shear magnitude increases, and the tropical cyclone vortex can develop in a more hostile environment. When the shear magnitude approaches the critical value under a given SST, the predictability of TC genesis will be quite low since small changes or errors in the shear magnitude can lead to dramatic differences in whether cyclogenesis proceeds or not.

Further analysis is performed in order to determine the dominating factor that leads to the above TC response to vertical wind shear. It is found that the variations in diabatic heat release, which lead to changes in the vortex mean circulation strength, produce a divergence in the timing of precession and vortex alignment. The dry air ventilation effect through boundary layer inflow is found to be not the main influence on the formation of the TC vortices in this study. It is shown, however, that the shear effect on the distribution and intensity of the convection is the primary reason for changes in the TC vortices during the precession cycle and among the different magnitudes of shear. The mechanism that influences these changes during the formation of TCs is the changes in the distribution and intensity of the diabatic heating, which subsequently affects the secondary circulation strength and the vortex mean circulation. The SST sensitivity experiments show that with higher SSTs, the amount of diabatic heating is much larger and the vortex intensifies much quicker than the lower SST experiments. When variations in the humidity of environmental air are introduced to the simulations, the results provide insight into how dry air influences the formation of the tropical cyclone. When dry air is placed in the surrounding area of the vortex, two effects on the TC are observed. First, the formation of convection outside the moist region (TC core) is unable to initiate. Second, the dilution of the diabatic heating (proxy for convection) occurs through the advection of the low θe air into the updrafts, which suppresses the convergence of angular momentum and reduces the vortex strength. Finally, this reduces the precession speed and slows the development of the TC.

This research studies the dynamics and thermodynamics of the TC vortex under different vertical wind shear, SST, and moisture content conditions, which has the practical predictability implication that in the real forecast cases the errors in the measurements of wind, SST or moisture can lead to failure of TC rapid intensification forecasts. In a future study of intrinsic predictability, we will focus on how small random initial-condition errors lead to dramatic differences in the predictability of RI onset under different sheared conditions. In addition, the sensitivity of the development of TCs to SST and environmental dry air will be explored in greater detail.

Acknowledgments
This work is partially supported by NASA under grant NNX12AJ79G, by NSF under grant 0840651, by Office of Naval Research under grant N000140910526, and by NOAA under the Hurricane Forecast Improvement Project (HFIP). Comments by Erin Munsell on an earlier version of the manuscript are greatly beneficial. Computing is performed at the Texas Advanced Computing Center (TACC).

References

Black, M. L., J. F. Gamache, F. D. Marks, C. E. Samsury, and H. E. Willoughby (2002), Eastern Pacific Hurricanes Jimena of 1991 and Olivia of 1994: The effect of vertical shear on structure and intensity, *Mon. Weather Rev.*, *130*, 2291–2312.

Braun, S. A., and L. Wu (2007), A numerical study of Hurricane Erin (2001). Part II: Shear and the organization of eyewall vertical motion, *Mon. Weather Rev.*, *135*, 1179–1194.

Braun, S. A., J. A. Sippel, and D. S. Nolan (2012), The impact of dry midlevel air on hurricane intensity in idealized simulations with no mean flow, *J. Atmos. Sci.*, *69*, 236–257.

Chen, S. S., J. A. Knaff, and F. D. Marks Jr. (2006), Effects of vertical wind shear and storm motion on tropical cyclone rainfall asymmetries deduced from TRMM, *Mon. Weather Rev.*, *134*, 3190–3208.

Corbosiero, K., and J. Molinari (2002), The effects of vertical wind shear on the distribution of convection in tropical cyclones, *Mon. Weather Rev.*, *130*, 2110–2123.

Davis, C. A., and D. A. Ahijevych (2012), Mesoscale structural evolution of three tropical weather systems observed during PREDICT, *J. Atmos. Sci.*, *69*, 1284–1305.

DeMaria, M. (1996), The effect of vertical shear on tropical cyclone intensity change, *J. Atmos. Sci.*, *53*, 2076–2087.

Dunion, J. P. (2011), Rewriting the climatology of the tropical North Atlantic and Caribbean Sea atmosphere, *J. Clim.*, *24*, 893–908.

Eliassen, A. (1951), Slow thermally or frictionally controlled meridional circulation in a circular vortex, *Astrophys. Norv.*, *5*, 19–60.

Emanuel, K. A. (1986), An air-sea interaction theory for tropical cyclones. Part I: Steady-state maintenance, *J. Atmos. Sci.*, *43*, 585–605.

Fang, J., and F. Zhang (2011), Evolution of multiscale vortices in the development of Hurricane Dolly (2008), *J. Atmos. Sci.*, *68*, 103–122.

Frank, W. M., and E. A. Ritchie (1999), Effects on environmental flow upon tropical cyclone structure, *Mon. Weather Rev.*, *127*, 2044–2061.

Frank, W. M., and E. A. Ritchie (2001), Effects of vertical wind shear on the intensity and structure of numerically simulated hurricanes, *Mon. Weather Rev.*, *129*, 2249–2269.

Franklin, J. L., S. J. Lord, S. E. Feuer, and F. D. Marks Jr. (1993), The kinematic structure of Hurricane Gloria (1985) determined form nested analyses of dropwinsonde and Doppler wind data, *Mon. Weather Rev.*, *121*, 2433–2451.

Fudeyasu, H., and Y. Wang (2011), Balanced contribution to the intensification of a tropical cyclone simulated in TCM4: Outer core spin-up process, *J. Atmos. Sci.*, *68*, 430–449.
Ge, X., T. Li, and M. Peng (2013), Effects of vertical shears and midlevel dry air on tropical cyclone developments, *J. Atmos. Sci.*, *70*, 3859–3875.
Gray, W. M. (1968), Global view of the origin of tropical disturbances and storms, *Mon. Weather Rev.*, *96*, 669–700.
Jones, S. C. (1995), The evolution of vortices in vertical shear. Part I: Initially barotropic vortices, *Q. J. R. Meteorol. Soc.*, *121*, 821–851.
Jones, S. C. (2004), On the ability of dry tropical-cyclone-like vortices to withstand vertical shear, *J. Atmos. Sci.*, *61*, 114–119.
Marks, F. D., Jr., R. A. Houze Jr., and J. F. Gamache (1992), Dual-aircraft investigation of the inner core of Hurricane Norbert. Part I: Kinematic structure, *J. Atmos. Sci.*, *49*, 919–942.
Montgomery, M. T., M. E. Nicholls, T. A. Cram, and A. B. Saunders (2006), A vortical hot tower route to tropical cyclogenesis, *J. Atmos. Sci.*, *63*, 355–386.
Munsell, E. B., F. Zhang, and D. P. Stern (2013), Predictability and dynamics of a non-intensifying tropical storm: Erika (2009), *J. Atmos. Sci.*, *70*, 2505–2524.
Nguyen, V. S., R. K. Smith, and M. T. Montgomery (2008), Tropical cyclone intensification and predictability in three dimensions, *Q. J. R. Meteorol. Soc.*, *134*, 563–582.
Nolan, D. S., and E. D. Rappin (2008), Increased sensitivity of tropical cyclogenesis to wind shear in higher SST environments, *Geophys. Res. Lett.*, *35*, L14805, doi:10.1029/2008GL034147.
Rappin, E. D., and D. S. Nolan (2012), The effect of vertical shear orientation on tropical cyclogenesis, *Q. J. R. Meteorol. Soc.*, *138*, 1035–1054.
Reasor, P. D., and M. T. Montgomery (2001), Three-dimensional alignment and corotation of weak, TC-like vortices via linear vortex Rossby waves, *J. Atmos. Sci.*, *58*, 2306–2330.
Reasor, P. D., M. T. Montgomery, and L. D. Grasso (2004), A new look at the problem of tropical cyclones in vertical shear flow: Vortex resiliency, *J. Atmos. Sci.*, *61*, 3–22.
Riemer, M., M. T. Montgomery, and M. E. Nicholls (2010), A new paradigm for intensity modification of tropical cyclones: Thermodynamic impact of vertical wind shear on the inflow layer, *Atmos. Chem. Phys.*, *10*, 3163–3188.
Rozoff, C. M., D. S. Nolan, J. P. Kossin, F. Zhang, and J. Fang (2012), The roles of an expanding wind field and inertial stability in tropical cyclone secondary eyewall formation, *J. Atmos. Sci.*, *69*, 2621–2643.
Sippel, J. A., and F. Zhang (2008), A probabilistic analysis of the dynamics and predictability of tropical cyclogenesis, *J. Atmos. Sci.*, *65*, 3440–3459.
Sippel, J. A., and F. Zhang (2010), Factors affecting the predictability of hurricane Humberto (2007), *J. Atmos. Sci.*, *67*, 1759–1778.
Stern, D. P., and F. Zhang (2013), How does the eye warm?. Part II: Sensitivity to vertical wind shear, and a trajectory analysis, *J. Atmos. Sci.*, *70*, 1849–1873.
Sun, Y. Q., Y. Jiang, B. Tan, and F. Zhang (2013), The governing dynamics of the secondary eyewall formation of Typhoon Sinlaku (2008), *J. Atmos. Sci.*, *70*, 3818–3837.
Tang, B., and K. Emanuel (2010), Midlevel ventilation's constraint on tropical cyclone intensity, *J. Atmos. Sci.*, *67*, 1817–1830.
Wang, Y. (2009), How do outer spiral rainbands affect tropical cyclone structure and intensity?, *J. Atmos. Sci.*, *66*, 1250–1273.
Wang, Y., and G. J. Holland (1996), Tropical cyclone motion and evolution in vertical shear, *J. Atmos. Sci.*, *53*, 3313–3332.
Xu, Y., and Y. Wang (2013), On the initial development of asymmetric vertical motion and horizontal relative flow in a mature tropical cyclone embedded in environmental vertical shear, *J. Atmos. Sci.*, *70*, 3471–3491.
Zhang, F., and J. A. Sippel (2009), Effects of moist convection on hurricane predictability, *J. Atmos. Sci.*, *66*, 1944–1961.
Zhang, F., and D. Tao (2013), Effects of vertical wind shear on the predictability of tropical cyclones, *J. Atmos. Sci.*, *70*, 975–983.